JBC RESEARCH ARTICLE

Conformational triggers associated with influenza matrix protein 1 polymerization

Received for publication, August 5, 2020, and in revised form, December 28, 2020 Published, Papers in Press, January 29, 2021,
https://doi.org/10.1016/j.jbc.2021.100316

Faiz Mohd-Kipli[1,2], Jolyon K. Claridge[1], Jelena Habjanič[1], Alex Jiang[1], and Jason R. Schnell[1,*]

From the [1]Department of Biochemistry, University of Oxford, Oxford, United Kingdom; and [2]Faculty of Science, Universiti Brunei Darussalam, Gadong, Brunei Darussalam

Edited by Karen Fleming

A central role for the influenza matrix protein 1 (M1) is to form a polymeric coat on the inner leaflet of the host membrane that ultimately provides shape and stability to the virion. M1 polymerizes upon binding membranes, but triggers for conversion of M1 from a water-soluble component of the nucleus and cytosol into an oligomer at the membrane surface are unknown. While full-length M1 is required for virus viability, the N-terminal domain (M1NT) retains membrane binding and pH-dependent oligomerization. We studied the structural plasticity and oligomerization of M1NT in solution using NMR spectroscopy. We show that the isolated domain can be induced by sterol-containing compounds to undergo a conformational change and self-associate in a pH-dependent manner consistent with the stacked dimer oligomeric interface. Surface-exposed residues at one of the stacked dimer interfaces are most sensitive to sterols. Several perturbed residues are at the interface between the N-terminal subdomains and are also perturbed by changes in pH. The effects of sterols appear to be indirect and most likely mediated by reduction in water activity. The local changes are centered on strictly conserved residues and consistent with a priming of the N-terminal domain for polymerization. We hypothesize that M1NT is sensitive to changes in the aqueous environment and that this sensitivity is part of a mechanism for restricting polymerization to the membrane surface. Structural models combined with information from chemical shift perturbations indicate mechanisms by which conformational changes can be transmitted from one polymerization interface to the other.

Influenza A virus (IAV) infections cause global health problems with cases of influenza-like illness typically in the tens of millions in a single season in the United States alone (1, 2). The efficacy of seasonal influenza vaccines ranges widely and is lower in young children and older adults motivating the search for antiviral drugs (3–5). The matrix protein 1 (M1) is the most abundant and most highly conserved protein of the influenza A virus (6, 7) making it a compelling antiviral target. M1 is a multifunctional protein involved in nuclear export of viral ribonucleoprotein (RNP), inhibition of viral transcription, recruitment of viral proteins during virus assembly and budding, and has a central role in virus morphology and stability (8). M1 expressed without other viral proteins forms virus-like particles (9). A feature of M1 that is critical for its role in virus morphology and stability and for incorporation into virus particles is its ability to self-assemble into long, helical polymers on the membrane surface (10–13). *In vitro*, oligomers form efficiently at neutral pH and disassemble at low pH (14, 15), consistent with RNP uncoating in acidic endosomes (16).

The M1 protein is 252 amino acids long and has a well-folded N-terminal domain (M1NT; residues 1–164) consisting of two 4-helix bundle subdomains (subdomain 1, helices 1–4; and subdomain 2, helics 6–9) connected by a crossover helix (helix 5) and a helical C-terminal domain (M1CT; residues 165–252). M1 oligomerization is promoted by membrane binding (17) and mediated by the N-terminal domain (18–20). Several high-resolution crystallographic structures of the N-terminal domain (M1NT) have been determined, all of which show the same overall architecture at neutral or low pH and with only modest structural changes. Variations in intermolecular contacts observed in crystal structures of the M1NT can provide insights into how M1 assembles at the membrane (Fig. 1*A*). More than half of the structures have "side-by-side," antiparallel dimers in the asymmetric unit in which helices 6 and 8 are at the dimer interface. The side-by-side dimer interface appears to be weak in solution but has been exploited for the development of protein cages (21). A "stacked" dimer arrangement of the M1NT is also observed frequently. In this stacked arrangement, loops at the ends of the M1NT helices form a dimer interface (12, 22). The parallel, stacked arrangement is consistent with the long, helical polymers of M1 observed in virions (11, 12), as well as more recent cryo-EM structures (13, 20). A similar stacked arrangement is adopted in the crystal lattice observed for the matrix protein from a distantly related orthomyxovirus, infectious salmon anemia (ISA) virus (23). In full-length structures of M1 from IAV and ISA virus, the M1CT is folded into a helical bundle, and both M1NT-M1NT and M1NT-M1CT intermolecular contacts are formed.

Several mechanistic aspects of M1 function are poorly understood, including the physical triggers responsible for converting M1 from a water-soluble factor in the nucleus and cytosol to an immobilized oligomer at the plasma membrane. The membrane-attached oligomerization state is difficult to

This article contains supporting information.

* For correspondence: Jason R. Schnell, Jason.Schnell@bioch.ox.ac.uk.

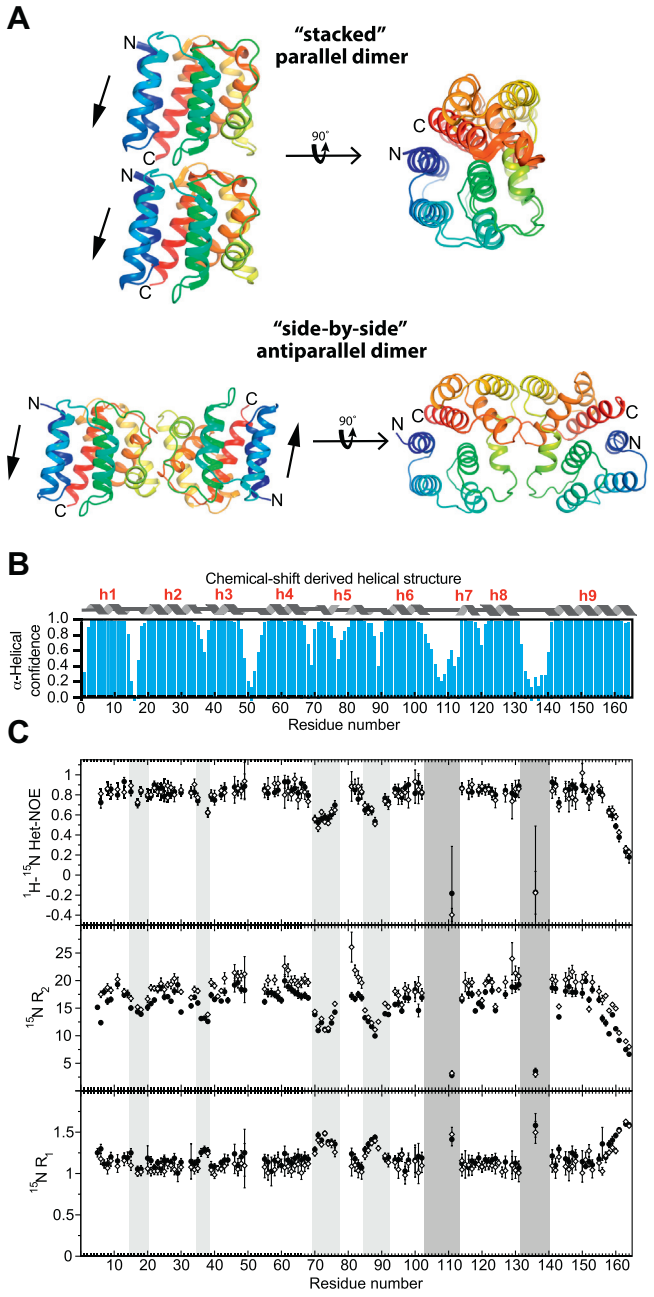

Figure 1. Crystallographic oligomerization modes, structure, and dynamics of the M1 N-terminal domain. *A*, common oligomerization modes for M1 observed in the crystallographic asymmetric units for the N-terminal domain. Shown at top is the stacked parallel dimer of 1EA3. At bottom is the side-by-side antiparallel dimer of 1AA7. *B*, secondary structure of the N-terminal domain of M1 in solution calculated from backbone and ^{13}Cβ chemical shifts using TALOS-N (53). *C*, {^{1}H,^{15}N}-heteronuclear NOEs and ^{15}N R_1 and R_2 relaxation rates for M1NT (*open symbols*) and the M1NT(L4Q) variant (*filled symbols*). Relaxation data indicate increased flexibility in the h1/h2 loop residues 15–20, h2/h3 loop residues 35–38, H4/H5 loop residues 70–77, and h5/h6 loop residues 85–92 (regions with *light shading*). Resonances corresponding to most of the h6/h7 loop (residues 103–113) and the h8/h9 loop (residues 132–140) were missing or too weak to assign (regions with *dark shading*), indicative of increased flexibility.

study at high resolution, and isolated full-length M1 is only weakly soluble as a monomer, although significant insights have been gained from low-resolution studies of the full-length monomeric protein in solution (14). In this study, we sought to identify the conformational triggers associated with M1 polymerization and the features that stabilize the oligomer interface. We show here that the M1NT conformation is sensitive to solution conditions including both pH and water activity. Combining our results with available structural information, we propose that conformational changes observed at one of the polymerization interfaces and at the M1NT subdomain interface prime the protein for polymerization.

Results

Characterization of the M1 N-terminal domain by NMR

The M1 N-terminal domain of influenza A recapitulates key features of full-length M1 oligomerization: membrane binding (18, 19), pH-dependent oligomerization (14, 15), and polymer assembly (20). We characterized an M1 N-terminal domain construct (M1NT) and found it was monomeric at concentrations of 50 μM, as determined by size-exclusion chromatography with multiangle light scattering (SEC-MALS) (Fig. S1), consistent with previous reports for both recombinant M1 (12) and M1 extracted from viruses (14). The NMR spectra of M1NT indicated a well-folded domain, as expected from crystallographic studies, and chemical shift assignments were possible for ∼85% of the backbone amides. Most signals for residues in the loops between helices 6 and 7 and between helices 8 and 9 were missing or too weak to assign suggesting they were dynamic. Chemical shift-based analyses of the observable resonances indicated that the secondary structure correlated well with what is seen in crystal structures (Fig. 1*B*).

The ^{15}N relaxation rates and heteronuclear overhauser effect (NOE) of M1NT and a more stable L4Q variant (M1NT(L4Q), see below) were measured to gain insights into flexibility (Fig. 1*C*). Decreased ^{15}N R_2 and {^{1}H-^{15}N} -heteronuclear NOEs relative to the helical regions indicated increased flexibility in the loops between helices 1 and 2 (residues 15–20) and helices 2 and 3 (residues 35–38) as well as the regions connecting the crossover helix 5 (residues 70–77 and 85–92). The relaxation properties of the glycines that could be assigned in the loops between helices 6 and 7 (residues 103–113) and between helices 8 and 9 (residues 132–140) confirmed that these regions were highly flexible.

To gain insights into whether the addition of native C-terminal domain sequence affects the M1NT conformation, we trialed purification and solubility of several M1 N-terminal constructs having increasing amounts of native C-terminal sequence. Solubility was assessed by UV absorbance after spin concentrating and qualitatively by monitoring for visible aggregates during sample concentration. The M1NT alone (residues 1–164) could be concentrated to ∼50 μM and was stable for ∼4 days at 30 °C and pH 7.0. The M1NT was approximately fourfold more soluble at pH 5.5. Ten constructs containing increasing amounts of C-terminal sequence, from residues 1–180 to residues 1–252 (full-length), were tested for solubility (residues 1–180, 1–186, 1–194, 1–201, 1–209, 1–224, 1–232, 1–236, 1–241, and 1–252). It was observed that the solubility at pH 7.0 decreased as the length of the C terminus increased. An M1(1–224) construct had a

concentration limit of ~20 μM at pH 5.5 and exhibited an intermediate propensity to self-assemble, in agreement with previous findings (24). Chemical shift perturbations (CSPs) within the M1NT indicated that addition of C-terminal sequence to residue 224 resulted in modest chemical shift changes. Soluble, monomeric samples of constructs longer than M1(1–224) could not be prepared at sufficient concentration for NMR studies.

The effects of pH on M1 conformation

Since the isolated N-terminal domain can self-associate in a pH-dependent manner similar to full-length ((15), and below), we sought to identify regions that were sensitive to pH. Differences in the chemical shifts of the M1NT monomer were measured from pH 3.5 to pH 7.0 (Fig. 2*A* and Fig. S2*A*). Perturbed residues for the pH range 5.5–7.0 are found in subdomain interface helices 1, 4, 7, and 9, as well as in helix 2 (Fig. 2*A*). As expected from typical histidine pK_a values, significant shifts were observed in H159 and H162. The resonance arising from H110 could not be reliably tracked in the titration, but perturbations observed over the pH range 5.5–7.0 in E114 (helix 7) and E6 (helix 1) are most likely due to titration of the H110 sidechain. Whereas chemical shift changes above pH ~5 are expected to be due primarily to titration of histidine sidechains, those below pH ~5 are expected to be due primarily to titration of glutamate and aspartate sidechains (25). Notable exceptions observed in M1NT were perturbations above pH 5.5 observed in E29 and D30, which are distant in structure from any histidines. The CSPs in E29 and D30 above pH 5.5 may be due to an unusually large pK_a shift in one of the two closely apposed carboxyls.

Perturbations at the subdomain interface suggested the possibility that pH affects the intramolecular interface between subdomain 1 (helices 1–4) and subdomain 2 (helices 6–9). The availability of several M1NT structures solved over a range of pH values provides an opportunity to test whether subdomain movements might be correlated with changes in pH. Six of the 11 M1NT coordinate files available are derived from wild-type A/Puerto Rico/1934 H1N1 (PR8) or wild-type A/Wilson-Smith/1933 H1N1 (WSN) strains, which differ in their M1NT sequences by just two conservative substitutions, and another four coordinate files are derived from WSN and contain a single G88E or G88R substitution (26, 27). Thus, in total there are 19 unique M1NT structures largely derived from WSN or PR8. Plotting the subdomain rotation between helices 1 and 4 and helices 6 and 9 relative to that of 1EA3 indicated a modest correlation with pH (R = 0.68). However, significantly greater variation in subdomain rotation was observed for structures without stacked dimers in the crystal lattice, and a strong correlation was detected for structures containing a stacked dimer arrangement (R = 0.81; 13 structures) (Fig. 2*D*). The stacked dimer is formed from two interfaces, and in subdomain 1 the interface is centered on I51, which is in a hydrophobic loop and protrudes into a shallow concave surface near T67 on the adjacent subunit. Thus, the structures can be further sorted according to whether the subdomain rotation correlates with packing at the I51 interface or the T67 interface. Stacked dimer formation at the I51 surface results in a very high correlation with pH (R = 0.96; eight structures) and may indicate that this interface is most sensitive to changes in electrostatics.

Early structural studies of the M1NT described a large tilt between crystalline stacked dimer subunits at low pH (22) (Fig. S2*B*). Seven stacked dimer arrangements of M1NT derived from either PR8 or WSN at six different pH values can now be quantified (Fig. 2*E*). The stacked dimer tilt angle was quantified by the subdomain 1 distances between I51 and T67. Plotting of the I51-T67 intermolecular distances against pH indicates a remarkably strong correlation (R = 0.98) (Fig. 2*E*) and confirms the earlier hypothesis (22), at least for crystalline M1NT in the stacked dimer arrangement. The tilted stacked dimer arrangements seen at lower pH may be related to the disrupted forms of oligomeric M1 after exposure to low pH (11, 22, 27, 28). The observation of CSPs at the subdomain interface in monomeric M1NT suggests that pH-dependent subdomain movements in the monomer might correlate with the geometry of the stacked dimer. Other factors however such as close approach of H159 and H162 at the end of helix 9 to H110 of an adjacent subunit are likely also important in regulating intermolecular domain tilt.

Sensitivity of M1NT to sterol compounds correlates with the propensity for oligomerization

Since association with membranes induces M1 oligomerization (17), we tested the effects of several membrane mimicking detergents on M1NT structure. M1NT was found to interact strongly with the single-chain detergents n-dodecyl-β-D-maltopyranoside (DDM) and Anzergent 3-14 (AZ314) (Fig. S3). Whereas addition of these detergents, even at low micromolar concentrations in the case of AZ314, resulted in severe narrowing of the signals and visible aggregates in the sample within minutes, M1NT was completely unperturbed by the addition of lauryl maltose-neopentyl glycol (LMNG). In contrast, the addition of the sterol-containing surfactant CHAPS induced highly specific CSPs and the protein remained stably solubilized (Fig. 3*A*). The backbone amides strongly perturbed by CHAPS included residues L4, G34, T67, and E141, which are part of a solvent-exposed N-terminal surface of M1NT formed by the N terminus and helical loops (Fig. 3, *B* and *C*) and are at one of the stacked dimer oligomerization interfaces (12, 29).

We then tested the effect of CHAPS on M1(1–224). The strongly perturbed and well-resolved resonance of T67 was used to quantify changes in the N-terminal surface patch in response to solution additives. The M1(1–224) construct exhibited a greater CSP upon addition of CHAPS than M1NT (Fig. 4*A*). In contrast, lowering the pH to 5.5, at which M1 does not efficiently oligomerize, decreased the CSP observed in T67. Thus, the sterol-induced perturbations of the T67 surface patch correlated with the propensity of M1NT to self-associate.

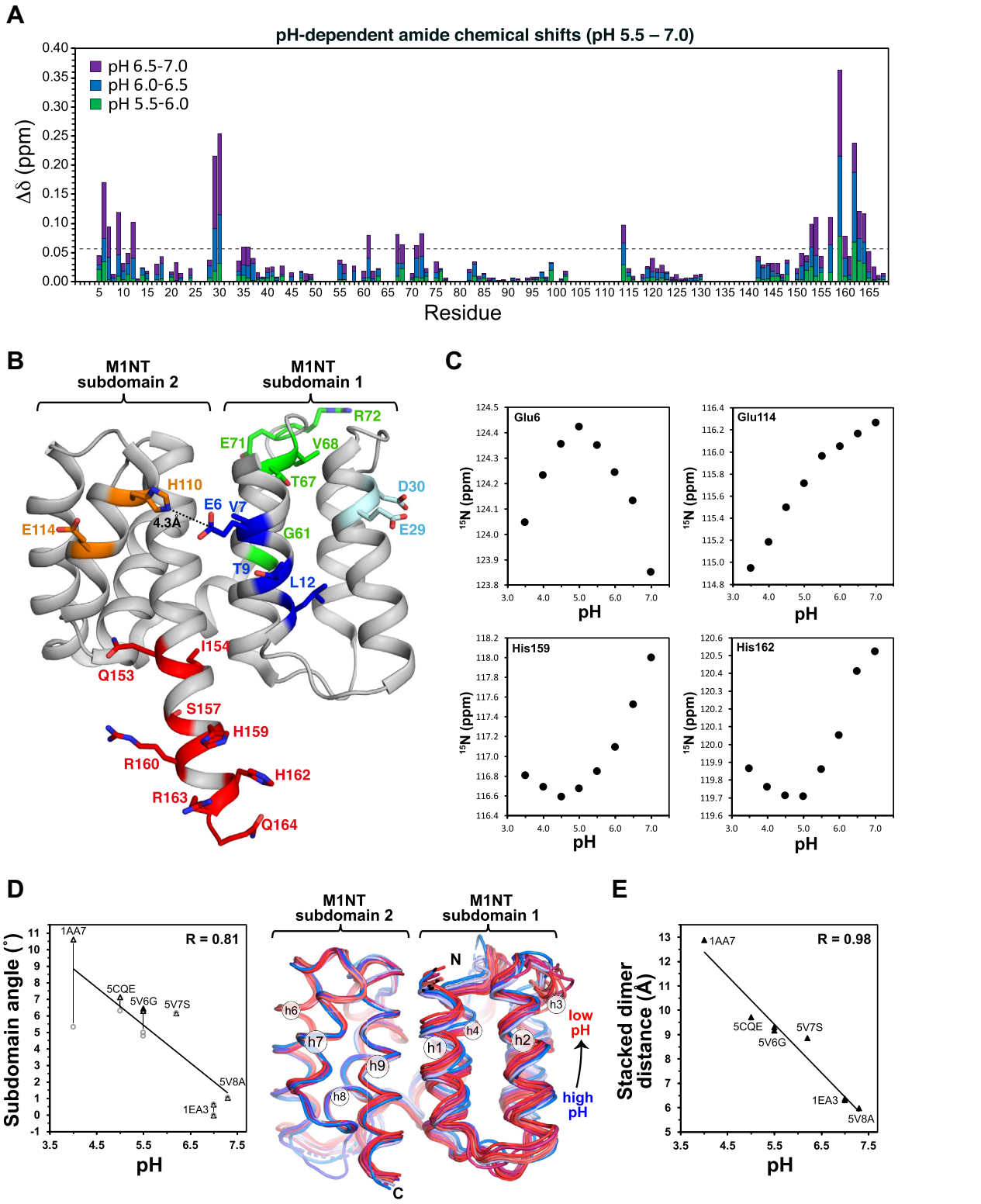

Figure 2. pH-dependent changes in the M1 N-terminal domain. *A*, the pH-induced chemical shift perturbations (CSPs) of M1NT prepared without the $(His)_9$ tag between pH 5.5 to 7.0. Spectra were recorded at 750 MHz and 25 °C. CSPs greater than one standard deviation (*dashed line*) were considered significant. *B*, ribbon diagram of the M1NT structure of Chiang *et al.* (27) (5V7S), which includes residues 159–163. The side chains of pH-sensitive residues determined in (*A*) are shown as sticks. Perturbed residues are found primarily in subdomain interface helices 1 (*dark blue*), 4 (*green*), 7 (*orange*), and 9 (*red*), as well as in helix 2 (*light blue*). The resonance arising from H110 could not be assigned but perturbations observed in E114 and helix 1 are presumed to be due to protonation of this residue over this pH range. *C*, amide ^{15}N chemical shift variation with pH for selected residues shown in (*B*). *D*, at left is an analysis of the subdomain angle (helices 1–4 *versus* 6–9; using 1EA3 chain A as the reference) in available structures derived from either A/Puerto Rico/8/1934 H1N1 (PR8) or A/Wilson-Smith/1933 H1N1 (WSN) strains as a function of the pH values at which they were determined. Data is shown for all structures for which stacked dimer interactions are observed. *Open triangles* indicate the subdomain angles of structures with I51 at the interface. *Open circles* indicate

CHAPS induces an extended conformation of T67 associated with a tightly packed stacked dimer

A stacked dimer arrangement is seen in several structures of the M1NT, with the neutral pH 1EA3 and 5V8A structures having the closest subdomain 1 intermolecular packing (Fig. 2*E*). The 1EA3 stacked dimer is associated with a uniquely extended conformation of the T67 backbone (Φ=−80°, ψ = 165°) compared with all other crystallographic structures (Φ = −93 ± 17°, ψ = −22 ± 21°), including 5V8a, in which the h4/h5 loop is not fully resolved (Fig. 4*C*). To test whether the CSPs observed upon addition of sterol-containing compounds are associated with a similar shift in the T67 backbone ψ angle, we measured $^{13}C'$ and $^{13}C\alpha$ chemical shifts in the absence and presence of CHAPS. For these studies we used the M1NT(L4Q) construct, which responds to the presence of CHAPS in a similar manner to the wild-type M1NT (Fig. S4) but is stable at higher concentration and for weeks at 30 °C in the NMR spectrometer. M1NT(L4Q) enabled us to record back-to-back triple-resonance experiments on the same sample with and without CHAPS. The chemical shift of T67 $^{13}C'$ was shifted 0.56 ppm upfield in the presence of CHAPS, indicating a more extended conformation, and confirming that sterols induce a shift in conformation of T67 in monomeric M1NT toward that seen in the stacked subunit arrangement of 1EA3.

Sterols affect M1 indirectly through water activity

Despite the apparently specific nature of the CHAPS-induced CSPs, intermolecular NOEs between protein and CHAPS could not be detected from either the backbone amides or the sidechain methyls. To understand which features of CHAPS were responsible for its effects on M1NT, we tested several other sterol-containing surfactants that differ in attached moieties. CHAPSO, cholate, and deoxycholate all produced similar CSPs to CHAPS (Fig. S5, *A*–*C*). In addition, saturation of sterol effects occurred at concentrations that correlated qualitatively with their critical micelle concentrations (cholate > CHAPSO > CHAPS >> deoxycholate) suggesting a primary role for monomeric sterols. Consistent with the similar effects between CHAPS/CHAPSO and cholate/deoxycholate, M1NT was unaffected by dimethylethylammonium propane sulfonate (NDSB-195) (Fig. S5*D*). These results indicate that some feature of the sterol rings was responsible for the effect on M1NT.

The tightly packed 1EA3 dimer structure was reported to be crystallized in the presence of isopropanol, which can strongly affect water activity (30). We therefore tested whether isopropanol can induce conformational changes in the N-terminal surface patch similar to sterols. Indeed, addition of 5% or 10% isopropanol to M1(1–164) induced CSPs in the same residues sensitive to CHAPS, and the individual shifts occurred in the same direction (Fig. 5*A*). Glycerol also reduces water activity and was used in the crystallization conditions for the ISA virus M1 protein (23). Addition of 5% or 15% glycerol resulted in similar chemical shift changes as CHAPS and isopropanol but with a reduced magnitude (Fig. 4*B*), consistent with its relatively smaller effects on water activity (31). Apart from containing hydroxyls, sterols, isopropanol, and glycerol are otherwise chemically very different, suggesting that their effects on M1NT structure are mediated indirectly and most likely through water activity.

CSPs were also monitored on addition of chaotropes or kosmotropes to explore the possible role of water structure in M1NT conformation. The chaotropes sodium isothiocynate and guanidine isothiocyanate at 0.5 M had negligible effects on NMR spectra of M1NT (Fig. S6, *A* and *B*). By contrast, the kosmotrope ammonium sulfate nonspecifically induced a large number of CSPs throughout the structure (Fig. S6*C*). The perturbations with ammonium sulfate were not strongly correlated with those seen with CHAPS and isopropanol but suggested that the N-terminal domain may also be sensitive to increases in water order.

Cholesteryl hemisuccinate and CHAPS induce M1NT oligomerization mediated by the stacked interface

While investigating sterol group effects, we sought to examine sterol compounds with fewer hydroxyls, including cholesterol. It was found that cholesteryl hemisuccinate (CHS) solubilized in CHAPS and added to M1NT or M1(1–224) at approximately stoichiometric concentrations led to loss of NMR signals from the M1NT at pH 7.0 but not at pH 5.5, which correlates with the expectations for a physiologically relevant association of M1NT into large assemblies (Fig. 6*A*). In contrast to detergents such as DDM and AZ314, which cause M1NT unfolding, many fewer signals were detectable on addition of CHS and CHAPS. In the case of M1(1–224), signals from the C-terminal region were detectable indicating that the C-terminal extension was largely unaffected. While samples became cloudy, precipitation was slow, occurring over 1–2 days. Increasing the temperature to 50 °C or reducing the pH to 5.5 was not sufficient to recover the M1NT signals. The heterogeneity and large size of the oligomers prevented reliable characterization by dynamic light scattering.

LMNG was unique among the detergents tested in that it did not interact with M1NT constructs on its own. It was therefore tested whether CHS solubilized in LMNG could also induce M1 self-association. LMNG-solubilized CHS did not perturb M1(1–164) signals. Finally, it was observed that another cholesterol compound, 25-hydroxycholesterol, combined with CHAPS did not induce oligomerization (Fig. S7). Thus, the specific combination of a sterol and CHS was required for M1 self-association.

subdomain angles of structures with T67 at the interface. 1EA3 and 5V8A are crystallized with a continuous stacked dimer arrangement and the duplicate structures for 1EA3 and 5V8A were not used in determination of the fitted line and indicated R value. At right are structural overlays of the structures aligned to the Cα of helices 6–9 of the first 1AA7 structure in order to show the pH-dependent relative subdomain rotation. Structures at pH 7 or above are colored in shades of *blue* (1EA3 (2), 5V8A (1)) and structures below pH 7 are colored in shades of *red* (1AA7 (2), 5CQE (2), 5V6G (4), 5V7S (2)). *E*, plot of the intermolecular Cα–Cα distance between I51 and T67 as a function of pH for the seven structures derived from A/Puerto Rico/8/1934 H1N1 or A/Wilson-Smith/1933 H1N1 that exhibit a unique stacked dimer interface. The PDB codes for each data point are indicated. The linear regression and the R-value are shown.

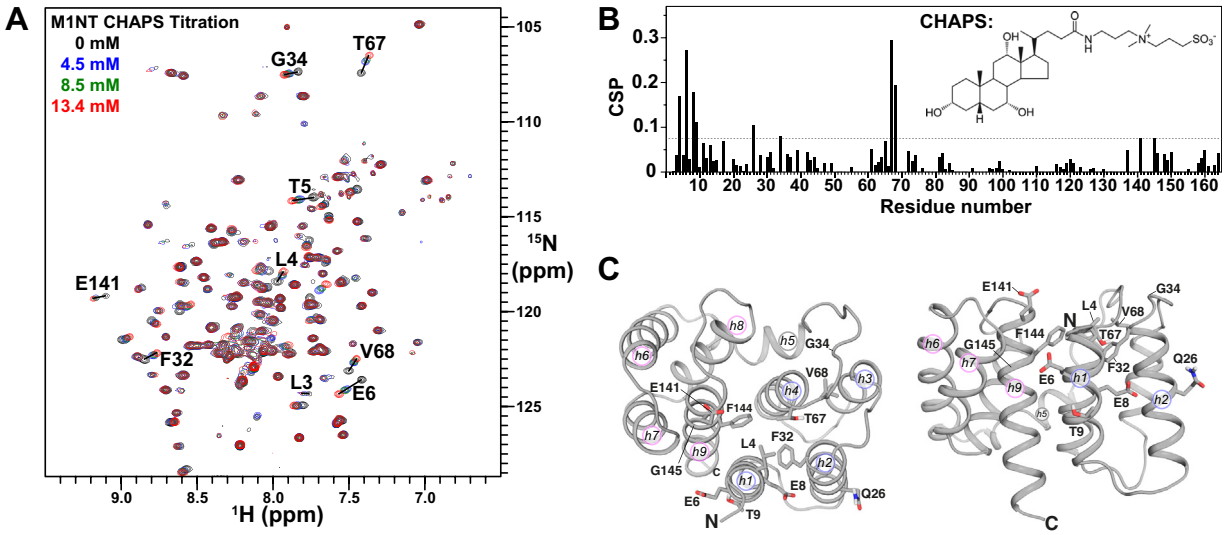

Figure 3. CHAPS-induced structural changes in the M1 N-terminal domain. *A*, spectral overlay of ^{15}N-labeled M1NT at 25 °C and pH 7.0 with increasing amounts of CHAPS indicating a saturable effect close to the critical micelle concentration of the detergent. *B*, per-residue chemical shift perturbations of M1NT at 13.4 mM CHAPS. (C) The residues with the largest chemical shift perturbations mapped to the 1AA7 structure of the M1NT. Perturbed residues are clustered in helix 1 (N-terminus), helix 2 (C-terminus), helix 4 (C-terminus), and helix 9 (N-terminus).

Since the residues L4, G34, T67, and E141 are strongly perturbed in the presence of sterols and also found at the stacked dimer interface of the 1EA3 structure (22), the following single-site substitutions were tested for CHS/CHAPS-induced complex formation: L4Q, L4K, T67S, and E141A. None of the mutations self-associated in the presence

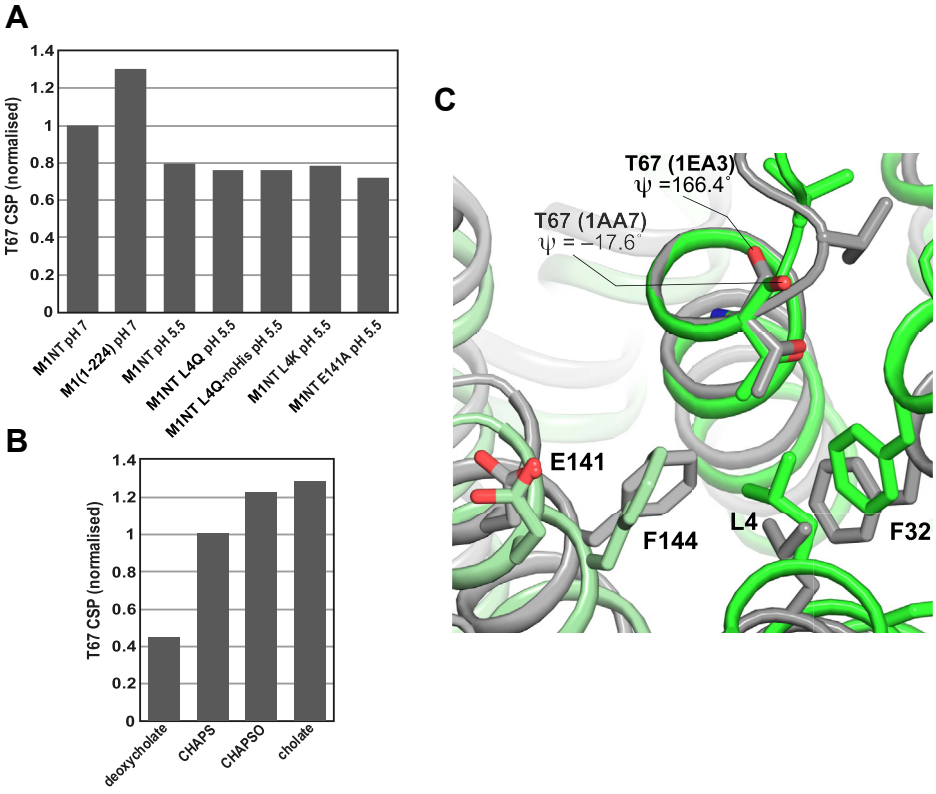

Figure 4. The effects of CHAPS and other sterols on the M1 N-terminal domain. *A*, the maximum chemical shift perturbation (CSP) due to sterols on the backbone amide of T67 in M1NT at pH 7.0. In both (*A*) and (*B*) the CSPs were calculated as a spectral distance with ^{15}N shifts underweighted fivefold relative to ^{1}H and normalized to the distance calculated for T67 of M1NT with CHAPS. *B*, the effect of construct length, pH, single-site substitutions, and removal of the histidine tag (noHis) on the maximum CSP of T67 due to CHAPS. *C*, structure showing the change in ψ backbone angle in T67, at the end of helix 4, between the low pH 1AA7 structure and the neutral pH 1EA3 structure of the stacked dimer. Both 1AA7 and 1EA3 are derived from the sequence of A/Puerto Rico/8/1934 H1N1. The side chains of residues L4, F32, E141, and F144, which are also perturbed upon addition of CHAPS, are shown as sticks. The two structures are superimposed over the Cα atoms of residues 65–67.

of CHS and CHAPS at pH 7 or pH 5.5 (Table 1 and Fig. 6*B*). The variant constructs remained soluble at higher concentrations than M1NT with wild-type sequence, and NMR spectra indicated that the substitutions largely affected the same residues perturbed by sterols but did not unfold the M1NT (Fig. S4*B*). The complementary stacked oligomer interface was tested with a charged polar substitution at I51, which packs against T67 at the stacked dimer interface seen in 1EA3 and 5V8A. This substitution also prevented CHS-induced M1NT oligomerization (Table 1).

We then tested by mutagenesis residues found at the side-by-side antiparallel dimer interface frequently seen in crystal structures of M1NT (Fig. 1*A*). A M93A/D94A double mutant within helix 6 was produced based on the large buried surface area for these residues at the side-by-side interface and the intermolecular D94 to K95/K98 salt bridge seen in the 1AA7 dimer. The M93A/D94A double mutant behaved similar to wild type, undergoing CHS-induced self-association at pH 7.0 consistent with this interface not being involved in the CHS-induced assembly (Fig. 6*B*).

Discussion

Membrane binding is known to accelerate M1 polymerization, but the mechanism underlying this process is unknown (17). The membrane-proximal environment exhibits strongly reduced water activity and increased water ordering (32, 33). Such features are known to affect solute hydration and therefore the energetics of protein–protein interactions (34). Sensitivity to water therefore can provide a mechanism for restricting protein–protein association at the membrane surface.

It was found here that the M1 N-terminal domain conformation is perturbed in a similar way by addition of different sterols, isopropanol, or glycerol despite these compounds being chemically very different. This suggests that the compounds act indirectly on M1 and most likely through a reduction in water activity (30, 31). Reduced water activity perturbs a network of mostly hydrophobic amino acids at one of the stacked dimer interfaces of M1NT. The perturbed residues are predominantly from the more highly conserved subdomain 1 (helices 1–4) of the M1NT (35). One of the effects of reducing water activity is an extension of the backbone of T67, which forms part of the tightly packed stacked dimer structure observed at neutral pH (12). T67 is part of a strictly conserved TLT sequence (residues 65–67) at the end of helix 4 (20, 35). It is therefore possible that these conformational changes have evolved to facilitate M1 polymerization in the unique aqueous environment of the membrane surface.

Although many residues perturbed by water activity are within subdomain 1, residues in helix 9 (E141 and F144) are also strongly perturbed. Helix 9 packs against helices 1 and 4 to form more than half of the subdomain interface, and perturbations here are consistent with movement between the subdomains. In addition, T67 and V68, which are very sensitive to reductions in water activity, are at the start of the loop between helix 4 and the subdomain linker helix 5. Crystal

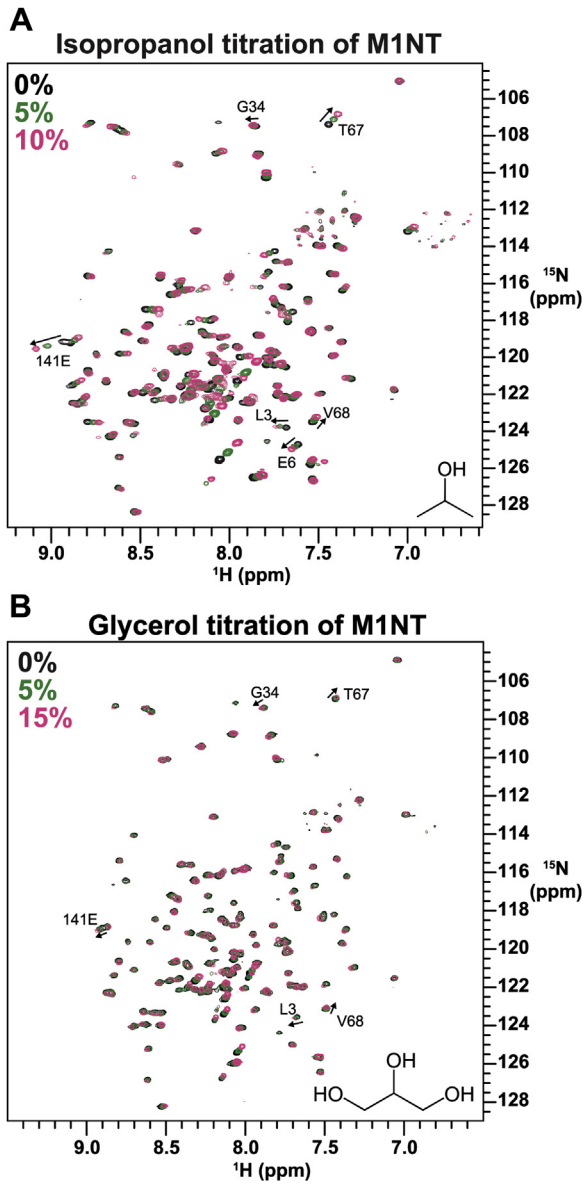

Figure 5. Isopropanol and glycerol affect the M1 N-terminal domain similarly to CHAPS. *A*, spectral overlay of M1NT alone (*black*) and in the presence of 5% (*green*) or 10% (*magenta*) glycerol. In (*A*) and (*B*), selected residue assignments and direction of peak movement are indicated. *B*, spectral overlay of M1NT alone (*black*) and in the presence 5% (*green*) or 15% (*magenta*) glycerol. All spectra were recorded at 25 °C and pH 5.5. Deuterium lock artifacts with glycerol were corrected for by aligning spectra on the crosspeak for residue T48.

structures confirm that the subdomains can rotate relative to each other (Fig. 2*D*). Subdomain rotation may also provide a mechanism for coordination between the two oligomerization surfaces. The overlap between the region perturbed by water activity and the region perturbed by pH, especially in helices 1 and 9, suggests that subdomain rotation may be generally involved in regulating M1 polymerization.

Allostery in M1NT is evident in comparing its response to the addition of native C-terminal sequence, which occurs at the polymerization interface on the other side from the T67 interface. In full-length M1, the C terminus adopts a stable tertiary structure and packs against the N-terminal domain of

an adjacent subunit to stabilize polymerization (23, 29). However, intermediate constructs that contain some C-terminal sequence but lack one or more of the C-terminal domain helices have a higher propensity to self-assemble (24). We observe here that the M1NT becomes more sensitive to changes in water activity with the addition of C-terminal sequence, despite the C terminus being unfolded and that this correlates with a greater propensity for self-association. The slight downfield shifting of $^{13}C'$ and $^{13}C\alpha$ chemical shifts at the end of helix 9 upon reduction of water activity (Fig. S4) is indicative of increased helix formation and suggests a possible mechanism for allostery between the C-terminal domain and the N-terminal polymerization interface of the M1NT.

It was discovered that the combination of CHAPS and CHS induced assembly of the M1 N-terminal domain into large complexes mediated by the same residues that are both sensitive to water activity and found at the stacked dimer interface. Oligomerization required the cholesterol derivative CHS and was not observed with 25-hydroxycholesterol, which lacks the negatively charged succinate. In addition, CHS in the presence of LMNG, which on its own does not interact with M1 or induce changes in the T67 surface, did not induce oligomerization. While influenza virions are highly enriched in cholesterol, M1 membrane binding does not appear to be influenced by its presence (36). Instead, it may be that the effect on oligomerization observed here is mediated by the negative charge of the CHS. The M1NT contains a strongly basic surface that mediates binding to negatively charged membranes (18, 36, 37), which may facilitate direct interactions with the CHS micelles. Results on M1NT variants are consistent with CHS-induced oligomerization occurring *via* the stacked dimer interface, but the relationship between binding to CHS and CHAPS micelles rather than physiological membranes is unknown. We note that cholate and deoxycholate produced perturbations similar to CHAPS and CHAPSO, did not appear to bind directly to the M1NT, and did not induce oligomerization despite being negatively charged. The positions of the charges on cholate and deoxycholate are very different from CHS and presumably also their positioning within a micelle. This suggests some dependence on the geometry of the charges for a direct interaction, but additional studies are required to understand the mechanism of CHS-induced oligomerization.

Based on our characterization of M1NT in solution and analysis of available M1NT structures, we propose that some specific features of the stacked dimer arrangement are relevant to the membrane-bound, polymerized form of M1. The extended conformation at T67 upon reduction in water activity correlates with what is observed uniquely in the 1EA3 stacked dimer subunits and may be required for close packing of subunits. Another interesting feature of 1EA3 is a single turn of 3_{10} helix in the helix 8/helix 9 loop, which is stabilized by a hydrogen bond between R134 and A137. Apart from G136, we were not able to detect and assign resonances in this region, but data from G136 suggests that the helix 8/helix 9 loop is disordered in the water-solubilized, monomeric form of M1 studied here. It nonetheless could provide important insights into stabilization of M1 polymers bound to negatively charged membranes. The presence of the 3_{10} helix is pH-dependent since it is formed in all six M1NT crystal structures determined at pH 7 or above and absent in four of the five structures determined below pH 7. The exception is 4PUS, which was crystallized at pH 4.7 but does not contain a stacked dimer interface. Formation of the 3_{10} helix results in the side

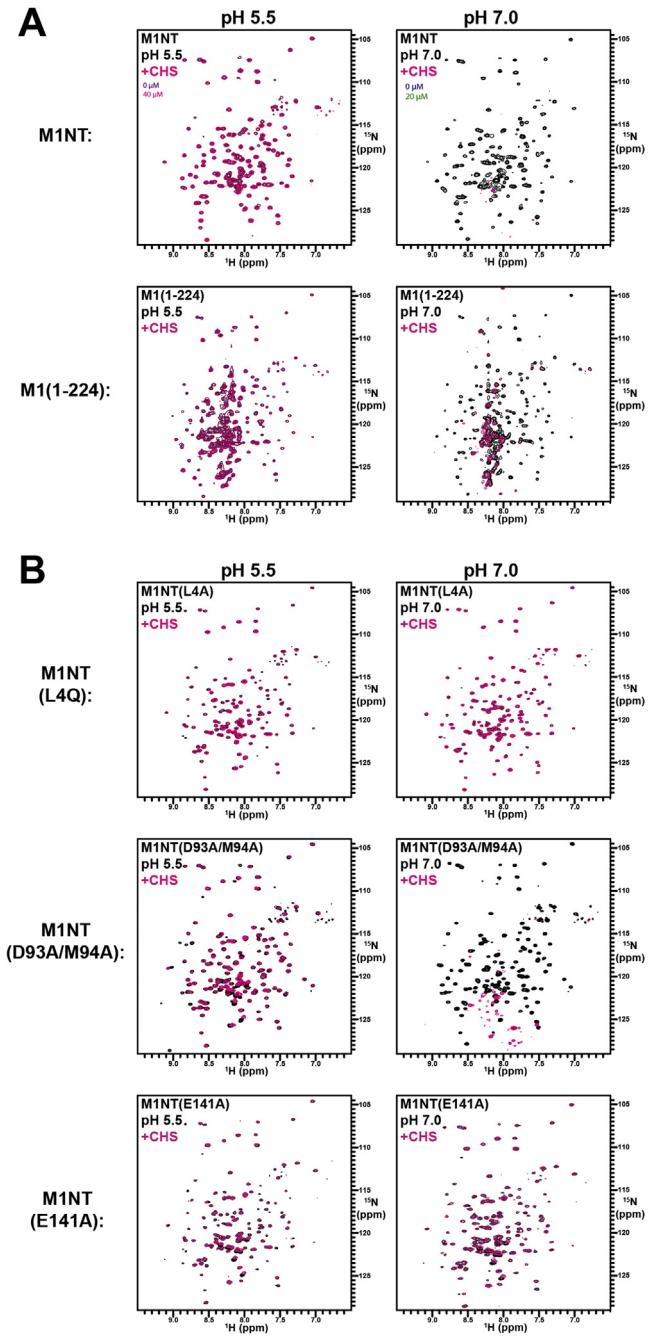

Figure 6. The effect of CHS on oligomerization interface mutants. *A*, overlays of M1NT and M1(1–224) constructs in the presence of saturating amounts of CHAPS before (*black*) or after (*magenta*) the addition of 10–40 μM CHS. In (*A*) and (*B*), samples were either at pH 5.5 (*left*) or pH 7.0 (*right*) and spectra were recorded at 25 °C. *B*, overlays of M1NT variants in the presence of saturating amounts of CHAPS before (*black*) or after (*magenta*) the addition of CHS.

Table 1
CHS/CHAPS-induced oligomerization of M1NT variants

Variant	M1NT construct	Oligomerization	
		pH 5.5	pH 7.0
Wild type	1–164	No	Yes
Wild type	1–224	No	Yes
L4Q	1–164	No	No
L4K	1–164	No	No
I51D	1–164	No	No
T67S	1–164	No	No
E141A	1–164	No	No
M93A/D94A	1–164	No	Yes

chain of R134 being flipped outward and contributing to the positively charged surface implicated in membrane binding (12, 19, 29, 38–40). Thus the 3_{10} helix results in large changes in the electrostatic profile of the membrane binding surface, which may be stabilized by interactions with negatively charged membranes or membrane mimetics (Fig. 7, *B* and *C*).

Formation of the 3_{10} helix also results in packing of M135 into a hydrophobic pocket formed by F62 and L66 of helix 4 (Fig. 7*B*). M135 is highly conserved in M1 from influenza A (41), and hydrophobic side chains are preferred at this position (35), but the relevance of the packing of M135 into the hydrophobic surface for the neutral pH stacked oligomer is unknown. Some CSPs were observed in L66, making it possible that the M135 pocket is sensitive to solution conditions. Further stabilization may come from closer contacts between residues 139/141 of the helix 8/helix 9 loop and 107/108 of the helix 6/helix 7 loop (Fig. 7*B*). These loops form a significant portion of the subunit interface, and flexibility observed here in the solublized monomer may contribute to regulating polymerization.

M1 contains a large number of phosphorylation sites (42), some of which have been implicated in M1 transport and signaling (43, 44). The results reported here suggest that phosphorylation may also play a role in regulating M1 polymerization. Regions identified as being involved in priming M1 for oligomerization can also be phosphorylated, including helix 1 (S2/T5 and T9/Y10) and the loop between helices 2 and 3 (T37) (42). Notably, the S2/T5 is on either side of L4, which was exploited here in the L4Q mutant used to stabilize the monomer. Another residue near to the conformational switch, S140, is strongly predicted to be phosphorylated by PKC, a kinase known to act on M1 (45).

In summary, we have found that the M1 N-terminal domain of an IAV protein is sensitive to water activity and propose that the protein senses a combination of both changes in water activity and the negative charges that are unique to the membrane surface. This is manifested as a repacking of the N-terminal subdomains and the oligomerization interfaces to facilitate polymer assembly. These conformational changes are allosteric, enabling conformational changes at one subunit surface to be transmitted to the C-terminal side. Such allostery may serve to propagate and possibly regulate the direction of polymerization. Despite diverse protein architectures, the matrix proteins of other enveloped viruses must be able to sense and respond *via* conformational changes to the unique local environment of the membrane surface. Similar to M1, polymerization of the ebolavirus matrix protein VP40 can be induced *in vitro* either in the presence of negatively charged membranes (46) or with solution additives such as urea (47) or dextran sulfate (48), which operate through unknown mechanisms. Our work here opens up the possibility that unrelated virus matrix proteins may also sense the unique aqueous environment of the membrane surface to regulate assembly.

Experimental procedures

Sample preparation

All M1 constructs were based on the A/England/250/2009(H1N1) sequence (J9UXB0) and codon-optimized for *E. coli* expression. All M1 constructs had a C-terminal 3C protease cut site followed by a $(His)_9$ tag. Constructs were cloned into the pCOLD II plasmid containing an ampicillin resistance gene. Plasmids were transformed into *E. coli* BL21(DE3) cells and grown in 2 L high-salt LB media to an OD(600 nm) of 0.5–0.8. Cells were cold shocked for 30 min on ice and left at 15 °C for 10–15 min. The cultures were spun down at 3000*g* for 15 min. Cell pellets were then resuspended in 1 L of 2x M9 minimal media containing either 1 g/l ^{15}N-labeled ammonium chloride or 1 g/l ^{15}N-labeled ammonium sulfate and 3 g/l ^{13}C-labeled glucose, and expression was induced with 1.5 mM IPTG. The cultures were left to grow overnight for 16–18 h and were then spun down at 4000*g* for 15 min. Pellets were resuspended in lysis buffer (20 mM Tris, 300 mM NaCl, 2 mM β-mercaptoethanol, 1 Roche EDTA-free inhibitor tablet per 50 ml lysis buffer, 1 mM EDTA, pH 7.5), and the cells were lysed using a high-pressure cell disruptor at 33 Kpsi. Cell debris was spun down for 15 min at 27,216*g*. The lysate was run over a 5 ml HisTrap FF column (GE Healthcare) and eluted with 300 mM imidazole. The eluted sample pH was adjusted to pH 5.0 and the salt concentration increased to 500 mM before it was concentrated for gel filtration using 10 kDa MWCO centrifugal concentrators up to a maximum of 150–200 μM. A Superdex Increase 200 10/300 GL column was equilibrated with running buffer (20 mM Tris, 500 mM NaCl, 1 mM EDTA, pH 5.5) before sample loading. The fractions with protein were collected and concentrated to 500 μl with 10 kDa MWCO centrifugal concentrators, buffer exchanged with NMR sample conditions (20 mM Tris, 50 mM NaCl, 2 mM β-mercaptoethanol, 1 mM EDTA, and pH 5.5). For samples at neutral pH, the concentrated sample was adjusted to pH 7.0 after concentration. Samples used for pH titrations were cleaved with 3C protease before gel filtration. Final yields for M1NT (residues 1–164) with the wild-type sequence and the M1NT(L4Q) variant were ∼1 mg and ∼2 mg, respectively, per liter of minimal media.

In vitro *oligomerization of M1*

CHS stock solutions (2%) were made up in 5% solutions of CHAPS. Solutions were sonicated until the solutions became translucent. Protein concentrations were 30–40 μM M1NT. Oligomerization was induced by the addition of 10–40 μM CHS.

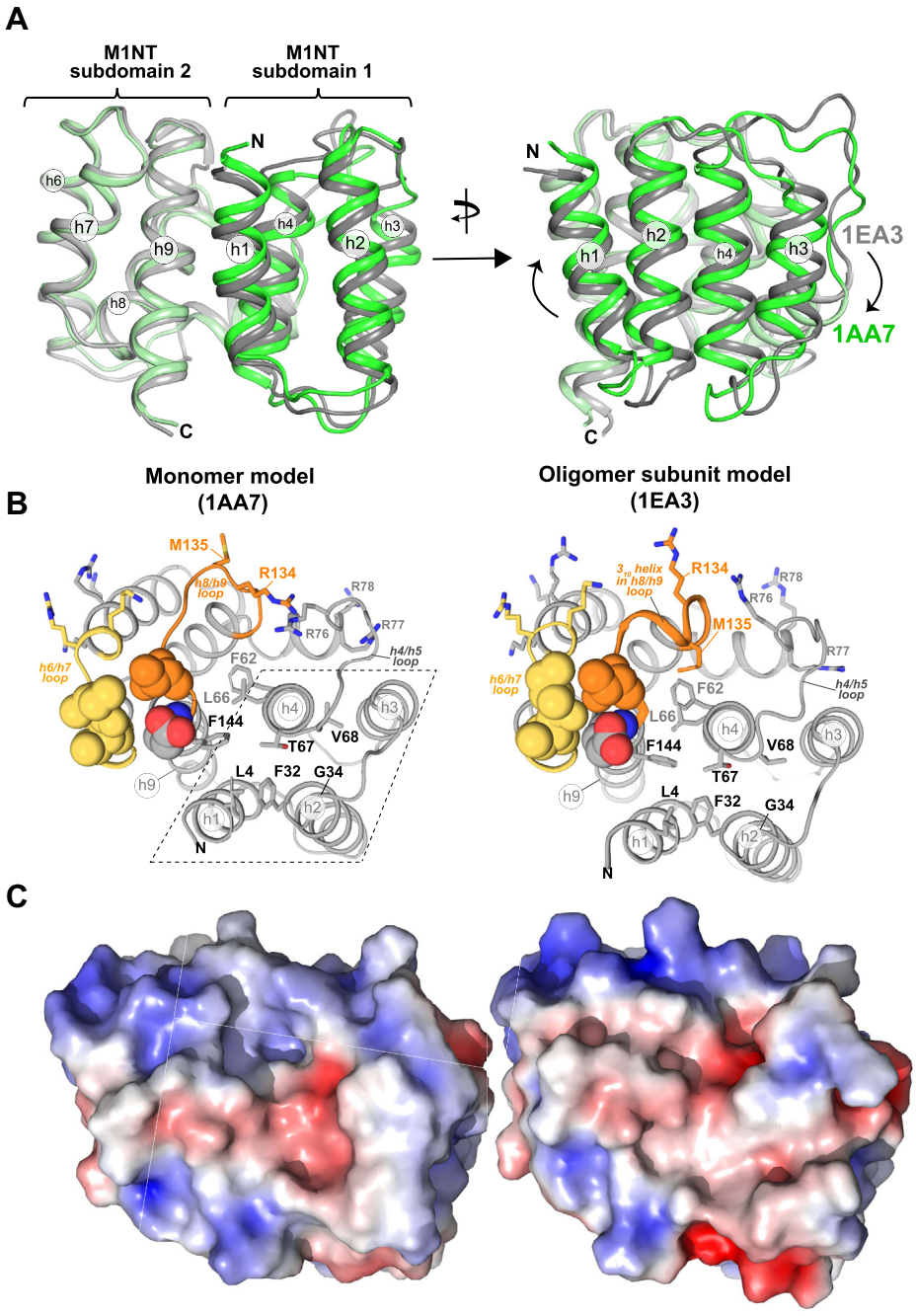

Figure 7. Conformational changes associated with the loosely stacked dimer 1AA7 and the tightly stacked dimer 1EA3. *A*, a comparison of a neutral pH, stacked dimer subunit from 1EA3, and a low pH structure from 1AA7. Both are derived from A/Puerto Rico/8/1934 H1N1. The structures are aligned on the Cα atoms of the C-terminal subdomain consisting of helices 6–9 to show the relative shift of the N-terminal subdomain consisting of helices 1–4. *B*, cartoon diagram of 1AA7 and 1EA3, which are models of the monomer and oligomer subunit structures. The view is onto the water-sensitive surface centered near T67 at the end of helix 4 (h4). The structures are oriented so that the membrane-binding surface is up. Subdomain 1 (helices 1–4) is shown within a *dashed-line parallelogram* in the structure on the left. Formation of a 3_{10} helix in residues 134–137 of the helix 8/helix 9 loop (h8/h9 loop; *orange*) of 1EA3 results in R134 flipping out at the membrane-interacting surface and M135 packing into the subunit interface. Closer packing between residues T139/E141 (shown as *spheres*) of the h8/h9 loop and residues I107/T108 (shown as *spheres*) of the helix 6/helix 7 loop (h6/h7 loop; *yellow*) may help reduce the loop mobility seen for the monomer in solution. *C*, surface representation of 1AA7 (left) and 1EA3 (right) colored according to electrostatic properties. The structures are shown in the same orientation as in the top panel. The conformational changes between 1AA7 and 1EA3 that are seen in T67/V68 and induced by CHAPS result in a rearrangement of the helix 4/helix 5 loop (h4/h5 loop) that remodels the oligomer interface. Large surface changes are also seen near the membrane binding surface with the formation of the 3_{10} helix of the h8/h9 loop in 1EA3.

NMR spectroscopy

Resonances of M1NT were assigned using BEST versions of 3D HNCA, HNCOCA, HNCACB, HNCOCACB, HNCO, and HNCACO spectra (49) at 750 MHz (^{1}H) collected on ^{13}C-^{15}N labeled protein (150 μM) at pH 5.5. Backbone amide assignments at pH 7.0 were obtained by titrating the pH from 5.5 to 7.0. T_1, T_2, heteronuclear NOE experiments were collected at 600 MHz (^{1}H) using ^{15}N-labeled M1NT(L4Q) at pH 5.5. NMR

data were processed using NMRPipe (50) and analyzed using CCPNmr Analysis (51) or CARA (52). Proton chemical shifts were referenced to DSS and ^{15}N and ^{13}C chemical shifts were referenced indirectly to proton.

Data availability

The assigned chemical shifts of M1NT have been deposited in the BioMagResBank (50,425). All other data described in the article are present in the main text, figures, and supplementary figures.

Acknowledgment—The Wellcome Trust is acknowledged for contributions to the upgrade of the 600 MHz NMR spectrometer used for data collection (WT094872MA).

Author contributions—F. M.-K. designed the experiments, prepared the protein constructs and samples, conducted chemical shift perturbation studies with additives, and analyzed the NMR data; J. K. C. designed and prepared the wildtype constructs and collected and analyzed the NMR data for wildtype chemical shift assignments; J. H. carried out the pH-dependent chemical shift experiments; A. J. prepared the protein samples and assisted with the additive chemical shift perturbation studies; J. R. S. designed the experiments, analyzed the data, and wrote the article.

Funding and additional information—This work was funded by a Chancellor's Scholarship to FMK and a grant from the UK Medical Research Council (L018578).

Conflict of interest—The authors declare that they have no conflicts of interest with the contents of this article.

Abbreviations—The abbreviations used are: CHS, cholesteryl hemisuccinate; CSP, chemical shift perturbation; DDM, n-dodecyl-β-D-maltopyranoside; IAV, influenza A virus; ISA, infectious salmon anemia; LMNG, lauryl maltose-neopentyl glycol; NOE, overhauser effect; RNP, ribonucleoprotein; SEC-MALS, size-exclusion chromatography with multiangle light scattering.

References

1. Rolfes, M. A., Foppa, I. M., Garg, S., Flannery, B., Brammer, L., Singleton, J. A., Burns, E., Jernigan, D., Olsen, S. J., Bresee, J., and Reed, C. (2018) Annual estimates of the burden of seasonal influenza in the United States: A tool for strengthening influenza surveillance and preparedness. *Influenza Other Respir. Viruses* **12**, 132–137
2. Reed, C., Chaves, S. S., Daily Kirley, P., Emerson, R., Aragon, D., Hancock, E. B., Butler, L., Baumbach, J., Hollick, G., Bennett, N. M., Laidler, M. R., Thomas, A., Meltzer, M. I., and Finelli, L. (2015) Estimating influenza disease burden from population-based surveillance data in the United States. *PLoS One* **10**, e0118369
3. Vemula, S. V., Sayedahmed, E. E., Sambhara, S., and Mittal, S. K. (2017) Vaccine approaches conferring cross-protection against influenza viruses. *Expert Rev. Vaccin.* **16**, 1141–1154
4. DiazGranados, C. A., Denis, M., and Plotkin, S. (2012) Seasonal influenza vaccine efficacy and its determinants in children and non-elderly adults: A systematic review with meta-analyses of controlled trials. *Vaccine* **31**, 49–57
5. Fineberg, H. V. (2014) Pandemic preparedness and response–lessons from the H1N1 influenza of 2009. *N. Engl. J. Med.* **370**, 1335–1342
6. Compans, R. W., Klenk, H. D., Caliguiri, L. A., and Choppin, P. W. (1970) Influenza virus proteins. I. Analysis of polypeptides of the virion and identification of spike glycoproteins. *Virology* **42**, 880–889
7. Ito, T., Gorman, O. T., Kawaoka, Y., Bean, W. J., and Webster, R. G. (1991) Evolutionary analysis of the influenza A virus M gene with comparison of the M1 and M2 proteins. *J. Virol.* **65**, 5491–5498
8. Kordyukova, L. V., Shtykova, E. V., Baratova, L. A., Svergun, D. I., and Batishchev, O. V. (2019) Matrix proteins of enveloped viruses: A case study of Influenza A virus M1 protein. *J. Biomol. Struct. Dyn.* **37**, 671–690
9. Gómez-Puertas, P., Albo, C., Pérez-Pastrana, E., Vivo, A., and Portela, A. (2000) Influenza virus matrix protein is the major driving force in virus budding. *J. Virol.* **74**, 11538–11547
10. Noton, S. L., Medcalf, E., Fisher, D., Mullin, A. E., Elton, D., and Digard, P. (2007) Identification of the domains of the influenza A virus M1 matrix protein required for NP binding, oligomerization and incorporation into virions. *J. Gen. Virol.* **88**, 2280–2290
11. Calder, L. J., Wasilewski, S., Berriman, J. A., and Rosenthal, P. B. (2010) Structural organization of a filamentous influenza A virus. *Proc. Natl. Acad. Sci. U. S. A.* **107**, 10685–10690
12. Arzt, S., Baudin, F., Barge, A., Timmins, P., Burmeister, W. P., and Ruigrok, R. W. (2001) Combined results from solution studies on intact influenza virus M1 protein and from a new crystal form of its N-terminal domain show that M1 is an elongated monomer. *Virology* **279**, 439–446
13. Peukes, J., Xiong, X., Erlendsson, S., Qu, K., Wan, W., Calder, L. J., Schraidt, O., Kummer, S., Freund, S. M. V., Kräusslich, H. G., and Briggs, J. A. G. (2020) The native structure of the assembled matrix protein 1 of influenza A virus. *Nature* **587**, 495–498
14. Shtykova, E. V., Dadinova, L. A., Fedorova, N. V., Golanikov, A. E., Bogacheva, E. N., Ksenofontov, A. L., Baratova, L. A., Shilova, L. A., Tashkin, V. Y., Galimzyanov, T. R., Jeffries, C. M., Svergun, D. I., and Batishchev, O. V. (2017) Influenza virus Matrix Protein M1 preserves its conformation with pH, changing multimerization state at the priming stage due to electrostatics. *Sci. Rep.* **7**, 16793
15. Zhang, K., Wang, Z., Liu, X., Yin, C., Basit, Z., Xia, B., and Liu, W. (2012) Dissection of influenza A virus M1 protein: pH-dependent oligomerization of N-terminal domain and dimerization of C-terminal domain. *PLoS One* **7**, e37786
16. Li, S., Sieben, C., Ludwig, K., Höfer, C. T., Chiantia, S., Herrmann, A., Eghiaian, F., and Schaap, I. A. (2014) pH-Controlled two-step uncoating of influenza virus. *Biophys. J.* **106**, 1447–1456
17. Hilsch, M., Goldenbogen, B., Sieben, C., Hofer, C. T., Rabe, J. P., Klipp, E., Herrmann, A., and Chiantia, S. (2014) Influenza A matrix protein M1 multimerizes upon binding to lipid membranes. *Biophys. J.* **107**, 912–923
18. Baudin, F., Petit, I., Weissenhorn, W., and Ruigrok, R. W. (2001) *In vitro* dissection of the membrane and RNP binding activities of influenza virus M1 protein. *Virology* **281**, 102–108
19. Höfer, C. T., Di Lella, S., Dahmani, I., Jungnick, N., Bordag, N., Bobone, S., Huang, Q., Keller, S., Herrmann, A., and Chiantia, S. (2019) Structural determinants of the interaction between influenza A virus matrix protein M1 and lipid membranes. *Biochim. Biophys. Acta Biomembr* **1861**, 1123–1134
20. Selzer, L., Su, Z., Pintilie, G. D., Chiu, W., and Kirkegaard, K. (2020) Full-length three-dimensional structure of the influenza A virus M1 protein and its organization into a matrix layer. *PLoS Biol.* **18**, e3000827
21. Lai, Y. T., Hura, G. L., Dyer, K. N., Tang, H. Y., Tainer, J. A., and Yeates, T. O. (2016) Designing and defining dynamic protein cage nanoassemblies in solution. *Sci. Adv.* **2**, e1501855
22. Harris, A., Forouhar, F., Qiu, S., Sha, B., and Luo, M. (2001) The crystal structure of the influenza matrix protein M1 at neutral pH: M1-M1 protein interfaces can rotate in the oligomeric structures of M1. *Virology* **289**, 34–44
23. Zhang, W., Zheng, W., Toh, Y., Betancourt-Solis, M. A., Tu, J., Fan, Y., Vakharia, V. N., Liu, J., McNew, J. A., Jin, M., and Tao, Y. J. (2017) Crystal structure of an orthomyxovirus matrix protein reveals mechanisms for self-polymerization and membrane association. *Proc. Natl. Acad. Sci. U. S. A.* **114**, 8550–8555
24. Zhang, K., Wang, Z., Fan, G. Z., Wang, J., Gao, S., Li, Y., Sun, L., Yin, C. C., and Liu, W. J. (2015) Two polar residues within C-terminal domain of

M1 are critical for the formation of influenza A virions. *Cell Microbiol* **17**, 1583–1593
25. Hass, M. A., and Mulder, F. A. (2015) Contemporary NMR studies of protein electrostatics. *Annu. Rev. Biophys.* **44**, 53–75
26. Xie, H., Lin, Z., Mosier, P. D., Desai, U. R., and Gao, Y. (2013) The compensatory G88R change is essential in restoring the normal functions of influenza A/WSN/33 virus matrix protein 1 with a disrupted nuclear localization signal. *J. Virol.* **87**, 345–353
27. Chiang, M. J., Musayev, F. N., Kosikova, M., Lin, Z., Gao, Y., Mosier, P. D., Althufairi, B., Ye, Z., Zhou, Q., Desai, U. R., Xie, H., and Safo, M. K. (2017) Maintaining pH-dependent conformational flexibility of M1 is critical for efficient influenza A virus replication. *Emerg. Microbes Infect* **6**, e108
28. Sha, B., and Luo, M. (1997) Structure of a bifunctional membrane-RNA binding protein, influenza virus matrix protein M1. *Nat. Struct. Biol.* **4**, 239–244
29. [preprint] Peukes, J., Xiong, X., Erlendsson, S., Qu, K., Wan, W., Calder, L. J., Schraidt, O., Kummer, S., Freund, S. M. V., Kräusslich, H.-G., and Briggs, J. A. G. (2020) The native structure of the full-length, assembled influenza A virus matrix protein, M1. *bioRxiv*. https://doi.org/10.1101/2020.06.24.168567
30. Zhu, H., Yuen, C., and Grant, D. J. W. (1996) Influence of water activity in organic solvent + water mixtures on the nature of the crystallizing drug phase. 1. Theophylline. *Inter. J. Pharm.* **135**, 151–160
31. Marcolli, C., and Peter, T. (2005) Water activity in polyol/water systems: New UNIFAC parameterization. *Atmos. Chem. Phys.* **5**, 1545–1555
32. Damodaran, S. (2015) Water at biological phase boundaries: Its role in interfacial activation of enzymes and metabolic pathways. *Subcell Biochem.* **71**, 233–261
33. Nagle, J. F., and Tristram-Nagle, S. (2000) Structure of lipid bilayers. *Biochim. Biophys. Acta* **1469**, 159–195
34. Parsegian, V. A., and Rau, D. C. (1984) Water near intracellular surfaces. *J. Cell Biol* **99**, 196s–200s
35. Hom, N., Gentles, L., Bloom, J. D., and Lee, K. K. (2019) Deep mutational scan of the highly conserved influenza A virus M1 matrix protein reveals substantial intrinsic mutational tolerance. *J. Virol.* **93**, e00161-19
36. Shilova, L. A., Knyazev, D. G., Fedorova, N. V., Shtykova, E. V., and Batishchev, O. V. (2017) Study of adsorption of Influenza virus matrix protein M1 on lipid membranes by the technique of fluorescent probes. *Biochemistry (Moscow)* **11**, 225–230
37. Ruigrok, R. W., Barge, A., Durrer, P., Brunner, J., Ma, K., and Whittaker, G. R. (2000) Membrane interaction of influenza virus M1 protein. *Virology* **267**, 289–298
38. Shishkov, A. V., Goldanskii, V. I., Baratova, L. A., Fedorova, N. V., Ksenofontov, A. L., Zhirnov, O. P., and Galkin, A. V. (1999) The *in situ* spatial arrangement of the influenza A virus matrix protein M1 assessed by tritium bombardment. *Proc. Natl. Acad. Sci. U. S. A.* **96**, 7827–7830
39. Das, S. C., Watanabe, S., Hatta, M., Noda, T., Neumann, G., Ozawa, M., and Kawaoka, Y. (2012) The highly conserved arginine residues at positions 76 through 78 of influenza A virus matrix protein M1 play an important role in viral replication by affecting the intracellular localization of M1. *J. Virol.* **86**, 1522–1530
40. Kerviel, A., Dash, S., Moncorgé, O., Panthu, B., Prchal, J., Décimo, D., Ohlmann, T., Lina, B., Favard, C., Decroly, E., Ottmann, M., Roingeard, P., and Muriaux, D. (2016) Involvement of an arginine triplet in M1 matrix protein interaction with membranes and in M1 recruitment into virus-like particles of the influenza A(H1N1)pdm09 virus. *PLoS One* **11**, e0165421
41. Darapaneni, V. (2015) Large-scale analysis of influenza A virus sequences reveals universally conserved residues of matrix proteins. *Am. J. Curr. Microbiol.* **3**, 1–13
42. Hutchinson, E. C., Denham, E. M., Thomas, B., Trudgian, D. C., Hester, S. S., Ridlova, G., York, A., Turrell, L., and Fodor, E. (2012) Mapping the phosphoproteome of influenza A and B viruses by mass spectrometry. *PLoS Pathog.* **8**, e1002993
43. Whittaker, G., Kemler, I., and Helenius, A. (1995) Hyperphosphorylation of mutant influenza virus matrix protein, M1, causes its retention in the nucleus. *J. Virol.* **69**, 439–445
44. Halder, U. C., Bhowmick, R., Roy Mukherjee, T., Nayak, M. K., and Chawla-Sarkar, M. (2013) Phosphorylation drives an apoptotic protein to activate antiapoptotic genes: Paradigm of influenza A matrix 1 protein function. *J. Biol. Chem.* **288**, 14554–14568
45. Reinhardt, J., and Wolff, T. (2000) The influenza A virus M1 protein interacts with the cellular receptor of activated C kinase (RACK) 1 and can be phosphorylated by protein kinase C. *Vet. Microbiol.* **74**, 87–100
46. Ruigrok, R. W., Schoehn, G., Dessen, A., Forest, E., Volchkov, V., Dolnik, O., Klenk, H. D., and Weissenhorn, W. (2000) Structural characterization and membrane binding properties of the matrix protein VP40 of Ebola virus. *J. Mol. Biol.* **300**, 103–112
47. Scianimanico, S., Schoehn, G., Timmins, J., Ruigrok, R. H., Klenk, H. D., and Weissenhorn, W. (2000) Membrane association induces a conformational change in the Ebola virus matrix protein. *EMBO J.* **19**, 6732–6741
48. Bornholdt, Z. A., Noda, T., Abelson, D. M., Halfmann, P., Wood, M. R., Kawaoka, Y., and Saphire, E. O. (2013) Structural rearrangement of ebola virus VP40 begets multiple functions in the virus life cycle. *Cell* **154**, 763–774
49. Schanda, P., Van Melckebeke, H., and Brutscher, B. (2006) Speeding up three-dimensional protein NMR experiments to a few minutes. *J. Am. Chem. Soc.* **128**, 9042–9043
50. Delaglio, F., Grzesiek, S., Vuister, G. W., Zhu, G., Pfeifer, J., and Bax, A. (1995) NMRPipe: A multidimensional spectral processing system based on UNIX pipes. *J. Biomol. NMR* **6**, 277–293
51. Vranken, W. F., Boucher, W., Stevens, T. J., Fogh, R. H., Pajon, A., Llinas, M., Ulrich, E. L., Markley, J. L., Ionides, J., and Laue, E. D. (2005) The CCPN data model for NMR spectroscopy: Development of a software pipeline. *Proteins* **59**, 687–696
52. Keller, R. (2004) *Optimizing the Process of Nuclear Magnetic Resonance Spectrum Analysis and Computer Aided Resonance Assignment*. Ph.D. thesis, Swiss Federal Institute of Technology Zurich
53. Shen, Y., and Bax, A. (2013) Protein backbone and sidechain torsion angles predicted from NMR chemical shifts using artificial neural networks. *J. Biomol. NMR* **56**, 227–241